Research Article

optica

Coherent laser ranging for precision imaging through flames

ERIC W. MITCHELL,[1] MATTHEW S. HOEHLER,[2] FABRIZIO R. GIORGETTA,[1] TORREY HAYDEN,[3] GREGORY B. RIEKER,[3] NATHAN R. NEWBURY,[1] ESTHER BAUMANN[1*]

[1] NIST 325 Broadway, Boulder, CO 80305, USA
[2] NIST Gaithersburg, MD 20899, USA
[3] CU Boulder, CO 80309, USA

*Corresponding author: baumann@nist.gov

Received XX Month XXXX; revised XX Month, XXXX; accepted XX Month XXXX; posted XX Month XXXX (Doc. ID XXXXX); published XX Month XXXX

Measuring the deformation of building elements engulfed by flames is essential in fire research to improve safety in the event of a fire. Ideally, the measurement system should be non-contact and able to range at the millimeter to meter scale with sub-mm precision and sufficient speed to capture temperature-induced deformations of the target object. To date, no ranging technology has been demonstrated that meets those requirements while imaging through flames. Here, we show that coherent laser detection and ranging (LADAR) can provide three-dimensional images of objects hidden behind methane or acetylene flames with sufficiently high precision to track their deformation. The heterodyne detection of coherent frequency modulated continuous wave (FMCW) LADAR allows the ranging signal to be detected in the presence of strong radiation of the flames. We measure three-dimensional point clouds of diffusely scattering complex surfaces with a precision of less than 30 μm at 2-meter stand-off distance, despite soot-induced signal loss and steering (refraction) of the ranging laser by the flames. Movies of the heat-induced surface deformation of objects illustrate the temporal performance. These data show that FMCW LADAR can quantify the deformation and movement of objects in fires, when non-contact shape measurements at stand-off distances of multiple meters are crucial.

OCIS codes: *(280.3400) Laser range finder; (280.2470) Flames; (030.1670) Coherent optical effects; (110.6880) Three-dimensional image acquisition*

http://dx.doi.org/10.1364/optica.99.099999

1. Introduction

In situ monitoring of deforming objects such as beams, columns or pipes engulfed by flames is essential to study the influence of fire on buildings and other structures and identify research, technology and regulatory needs to improve structure performance in the event of a fire [1–5]. Measurements on the millimeter to meter scale with sub-mm precision are typically required, and are challenging to perform through a fire's extreme environmental conditions. Glowing hot structural materials and gas temperatures in excess of 1200°C severely limit direct (contact) measurement using electromechanical sensors and traditional imaging is hindered by fire spectrum interference [6]. So far, no method has been demonstrated that excels at both seeing through flames and offering high precision at larger stand-off where photon efficiency is crucial.

Contactless optical three-dimensional (3D) distance metrology is used in many fields including precision machining, part inspection, and manufacturing [7–9]. There are numerous approaches to capture a 3D shape with light, including incoherent and coherent methods. Each method varies in performance and requirements in terms of precision, acquisition rate, and lighting condition. Structured light [10] offers very high update rates, enabling for example the capture of changes in facial expressions, but requires a well-controlled environment and short stand-off distances. It is thus not well-suited to measure small deformations of objects situated many meters away from the measurement setup, especially when hidden behind flames and smoke [11]. Ref. [12] successfully applied digital holography through smoke and flames using long wavelength illumination at 10.6 μm, but required a specialty camera sensitive to 10.6 μm and high-power laser illumination. Recently, single laser triangulation with blue (405 nm) light successfully ranged through small (< 4 kW) natural gas flames [11],

but this method is generally applicable only at stand-offs of 10 mm to 1 m [9]. Coherent cw laser ranging offers high photon efficiency to support large stand-off distances at modest output power levels and strong rejection of stray light from flames [13]. In this paper, we demonstrate that frequency modulated continuous wave laser detection and ranging (FMCW LADAR) [14–16], which is essentially identical to swept-laser optical coherence tomography [17], can successfully capture 3D point clouds of deforming objects through flames, with traceable precision and at sampling rates sufficient for most structural fire engineering applications.

FMCW LADAR has many attractive features for imaging through flames. The heterodyne detection used in FMCW LADAR is robust against background radiation from the fire, even when operating at 1560 nm (corresponding to the peak radiance wavelength of a 1900 K blackbody, close to typical flame temperatures). FMCW LADAR is very sensitive (photon efficient), enabling ranging to a diffusely scattering surface in or behind a sooty flame. It can operate at large stand-off distances, which allows the user to place the measurement setup out of harm's way. The setup can also be placed in a semi-transparent protective enclosure, as FMCW LADAR allows masking and filtering of signals based on distance. Finally, the combination of fiber-optic delivery and simple single-element photodetection allows for versatile, compact configurations.

Here, we show that FMCW LADAR can successfully retrieve 3D point clouds at high ranging precisions (of 30 µm or better) when ranging through the highly turbulent environment, with strong refractive index variations, scattering and attenuation encountered with flames. We quantify the effects of both a low-soot yield methane flame and a sooty acetylene flame on the FMCW LADAR ranging precision. We show that the update rate is sufficient to capture non-reversible surface deformations induced by the heat of the flames at 30-µm ranging precision by acquiring movies of melting chocolate, an Aluminum step block, and a geometrically-complex plastic toy. Finally, we discuss scaling to larger structure fires.

2. Measurement setup

Figure 1 shows an overview of our ranging setup. The light from the FMCW LADAR module is output in a polarization maintaining (PM) fiber and launched into free-space through a physical contact (PC) fiber connector. This connector doubles as a 4 % reflector, generating the local oscillator (LO), or fixed reference path, light. A fraction of the launched light is reflected by the target and captured back into the single mode PM fiber, after which it is heterodyned with the LO.

In FMCW, the laser light has a constant optical frequency chirp. As a result, the heterodyne signal is modulated at a radio frequency (RF) given by the product of this frequency chirp and the delay time τ between target and LO reference reflection. Since the chirp is known, the measured RF modulation frequency gives the delay time τ and finally the range $R=c/(2n)\tau$, where c is the speed of light and n is the refractive index of the optical path.

We use a commercial FMCW LADAR unit from Bridger Photonics, Inc.[1] (model SLM-IM) with an update rate of 1 kHz (upgradeable to 4 kHz). Its ~25 mm diameter, 17 mW beam is launched and focused to 300 µm $1/e^2$ diameter at 2 meters stand-off by an adjustable beam expander. For these experiments, the optical beam passes through a diffusion flame that is ~50 mm thick and ~0.3 m - ~ 0.5 m tall. The flame is generated from methane or acetylene gas with a flow rate of ~20 l/min through a slot burner of dimensions 310 mm × 15 mm. The

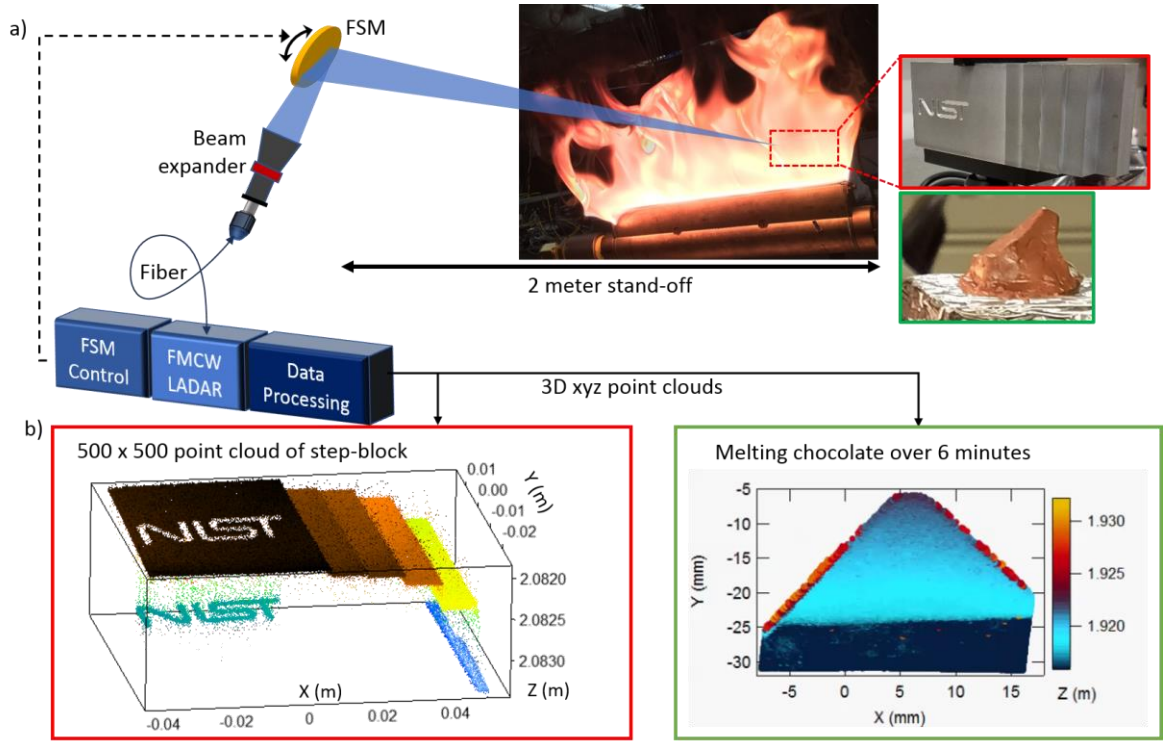

Figure 1: a) Experimental ranging setup. A target obstructed by flames (depicted is an acetylene flame) is scanned with a FMCW LADAR. The target is placed ~ 0.5 m behind this wall of flames, the total stand-off is 2 meters. Range measurements are taken continuously at a 1 kHz update rate. A fast steering mirror (FSM) sweeps the beam across the target and the resulting 3D point cloud is then transformed to obtain Cartesian xyz points. b) xyz 3D point clouds. Left panel: machined aluminum step-block. Right panel: video (see visualization 1) of a piece of chocolate, showing the deformation due to the flame heat (the frame rate is accelerated 60x to 1 Hz).

[1] Certain commercial products are identified in this paper to specify the materials used and the procedures employed. In no case does such identification imply endorsement or recommendation by the National Institute of Standards and Technology, nor does it indicate that the products are necessarily the best available for the purpose.

target is placed ~ 0.5 m behind this 'wall of fire'. A 3D point cloud is acquired by scanning the LADAR beam across the target using a fast steering mirror (FSM). Each range measurement is corrected for geometrical distortions introduced by the FSM to give a xyz point cloud in Cartesian coordinates [15]. The sampling density was chosen according to the desired area coverage and precision requirements. Figure 1b) shows two 3D point clouds; On the left, a 500 × 500 point cloud of a machined aluminum step-block acquired in 250 seconds and on the right 250 × 250 voxel/frame video of a piece of chocolate melting due to the heat of the flame. The video covers ~ 6 minutes at a frame rate of one frame per 60 seconds.

3. FMCW LADAR: Oversampling, frame rate, achievable range precision

In this section, we first review the performance in the absence of flames including lateral sample spacing, frame rate, range precision and measurement depth. The frame rate of a scanning 3D ranger is the number of points per image multiplied with the fixed single-point measurement time. The choice of a frame rate therefore involves trade-offs between covered area, spatial resolution (lateral sample spacing), time resolution, and range precision. In this work, all 3D images were acquired using a triangular scanning pattern. The single-point measurement time was 1/1 kHz = 1 ms. This 1 kHz update rate is not fundamental and is expected to increase at least fourfold in the future.

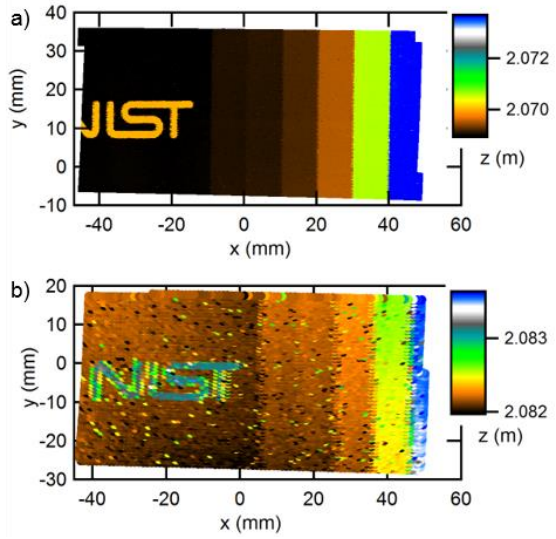

Figure 2: 3D images of the step-block. a) 10^6 point cloud, corresponding to 16 minutes/frame, b) 10 000 point cloud at 10 seconds/frame. Note that the mapped area on the step-block differs slightly.

Figure 2 shows two 3D images of the same 4200 mm² surface, for 10^6 points at a 1 mHz frame rate (panel a) and for 10 000 points at a 0.1 Hz frame rate (panel b). While the reduced number of measurements covering the surface in b) gives a noisier image, most of the target's steps (varying from 30 μm to 3 mm) are still visible.

As discussed in Ref. [15], speckle noise and other effects can lead to range outliers. In general, following [15], we limit valid range measurement to a signal-to-noise ratio (SNR) of at least 30 dB, which masks bad measurements caused for example by increased speckle phase noise [18], sharp edges of the target, or distances well outside of the focused beam's Rayleigh range. For our optics, the Rayleigh range was about 50 mm and, as a general rule of thumb, we then require the target depth variations to be within the corresponding confocal range of ~100 mm for a "sharp" image.

To quantify the measurement precision, we calculate the 1-σ standard deviation of a cross-section along the x-axis for a flat portion of the aluminum step block shown in Figure 2 (after applying a linear fit to remove any overall slant). As discussed in Ref. [18], the precision will depend on the scan speed (or lateral sample spacing) because of moving speckle noise. For example, comparing a densely sampled image to a sparsely sampled one, as shown in Figure 2, the precision deteriorates from 20 μm (including range deviations of a not perfectly flat surface) to 100 μm, and it becomes hard to quantify the smallest step of 30 μm. In general, to avoid excessive speckle noise, the scanning measurement beam should move by less than half a beam diameter during a single measurement. As discussed below, this same speckle noise will couple angular beam jitter induced by the flames with a slight decrease in measurement precision.

4. 3D Imaging of complex and deforming objects through flames

We now consider 3D images obtained while ranging through flames. Both methane and acetylene diffusion flames are used to test ranging under different flame conditions. Compared with clean-burning methane, acetylene produces a higher temperature, more luminous, sooting flame. Figure 3 shows two xyz 3D false-colored images of the aluminum step-block with 1 million pixels per image, acquired in 1000 s (highly oversampled to avoid additional moving speckle noise as described above). Figure 3a) is taken without flame, while Figure 3b) is obtained while ranging through a ~50 mm thick acetylene flame with the block almost completely obscured by the flame visually (shown in Figure 1a)). As seen in Figure 3, the two 3D images appear nearly identical.

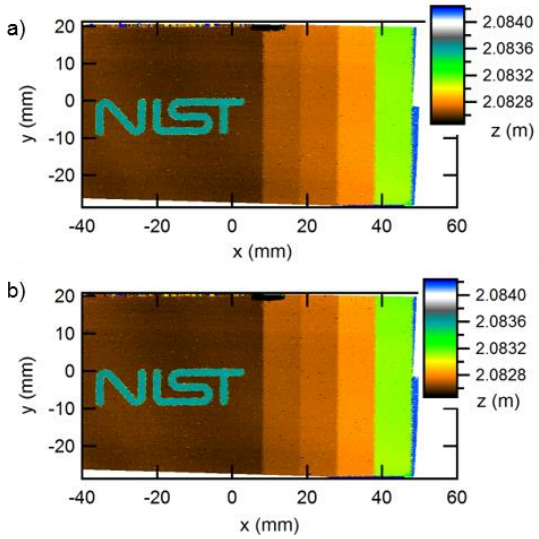

Figure 3: 3D xyz point cloud of the aluminum step-block where z is indicated in false color. A linear slope is removed from both images. a) 3D image with no flame in the ranging path. b) 3D image with block placed 0.5 m behind a ~50-mm thick acetylene flame.

Further analysis of the two images reveals a slight deterioration caused by the acetylene flame. First, the number of points that are removed because their SNR is below 30 dB increases from 1.66 % to 2.43 %, which we attribute to increased soot scattering and attenuation. Second, there is a small percentage (0.02 %) of additional larger range outliers which deviate by more than ±100 μm from an otherwise mostly flat measured surface. (These are masked out by thresholding.) Third, the ranging precision decreases from 20 μm to 31 μm. This slightly degraded precision and increase in large range outliers are attributed to beam deflection in the flame in conjunction with speckle as is described in the next section.

Figure 4 shows a plastic skeleton placed behind a methane flame. While the skeleton is obscured by the flame in the video (Figure 4a)), the

FMCW LIDAR is able to accurately measure its complex 3D shape Figure 4b), showing details of the ribcage and hips.

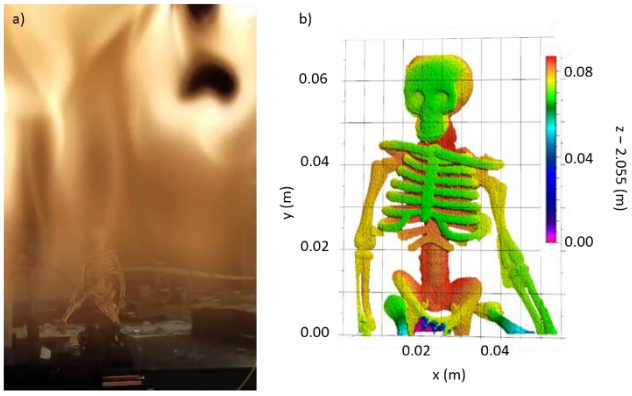

Figure 4: a) Video of methane flame and picture of a plastic skeleton, visualization 2. b) False-colored rendered 3D 1-million-point cloud of the plastic skeleton as mapped in 3D through the flame.

Finally, to investigate the capabilities of the FMCW LADAR system to capture deforming objects, a piece of chocolate is placed behind a methane flame, where it deforms slowly due to the heat from the flame (Figure 5). The process is captured by both 2D video (at an oblique angle not traversing the flame (Figure 5b) and FMCW LADAR (through the flame Figure 5c). Each LADAR frame consists of 7500 points giving a frame rate of 0.13 Hz, sufficient to capture the chocolate deformation process. 35 LADAR frames are recorded in just over 4 minutes. Future increased frame rate of the FMCW LADAR to 4 kHz and beyond will further improve the 3D video time resolution.

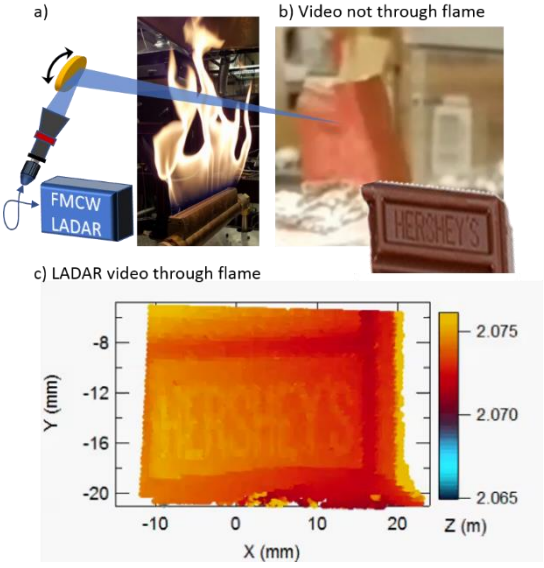

Figure 5: a) Sketch of ranging beam measuring melting chocolate through a methane flame. b) Picture of the chocolate bar and video (not through flame, visualization 3) of melting chocolate bar, visualization 4. c) LADAR video at a measured frame rate of 0.13 Hz (sped up to 10 Hz).

5. Impact of flame on ranging

To analyze the flame's influence on ranging in more detail, we perform range measurements to a diffusely scattering aluminum target over many minutes without scanning the beam (i.e. with the FSM at a fixed position). The flame affects the measurement in several ways. First, the flame causes a lensing effect that deflects the laser beam. Second the gas refractive index changes with temperature, leading to changes in delay-time and thus range measurements. Third, soot generated by the flame scatters and attenuates the laser light. In the following subsection, these effects are discussed in more detail and their effect on the ranging in terms of single-measurement precision, precision after averaging (Allan deviation) and the power spectral density (PSD), where the natural oscillation or flickering of a flame is evident.

A. Beam deflection through flame

In a first experiment, we quantify the effect of beam deflection on ranging through a flame. We first quantify the angular deflection caused by the flame. As shown in Figure 6a) the target is replaced by an indium gallium arsenide (InGaAs) focal plane array (FPA) with a 12.5 µm pixel pitch and a 60 Hz frame rate, situated about 0.4 m behind the flame at the target position. The laser beam is imaged by the FPA, and its x/y center coordinates are then calculated by fitting a 2D Gaussian to each FPA image from which we calculate the angular deflection. As shown in Figure 6b), the beam suffers a maximum angular deflection of ±0.75 mrad with a standard deviation of 0.1 mrad in both x and y direction.

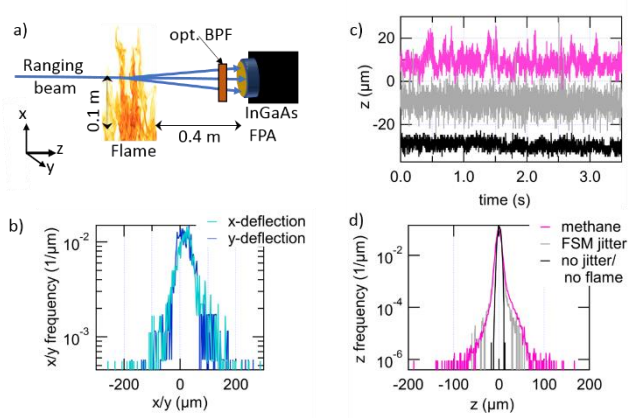

Figure 6: Effect of flame-induced beam deflection on ranging. a) Schematic of beam deflection measurements through a methane flame as captured by an InGaAs focal plane array (FPA). To avoid FPA saturation by the flame, light outside the FMCW LADAR bandwidth is blocked by an optical band-pass filter (BPF) centered at 1560 nm. b) Distribution of lateral beam-deflection in the x/y plane extracted from the FPA images. c) 3.5-second-long example of range measurements to a diffusely scattering aluminum target through a methane flame. Data is shown for a flame without scanning (pink), for no flame without scanning (black), and for no flame but while applying an angular jitter via the FSM equivalent to that induced by the flame (gray), d) corresponding range distribution (z-direction).

The angular deflection of the beam couples to increased ranging noise in two ways. Based on geometric considerations, if the target is slanted relative to the ranging beam (i.e. $\phi_t \neq 90°$), beam deflection will result in significant variation in measured range of $\delta r = r_0\left(\sin(\phi_t)/\sin(\phi_t + \phi_f) - 1\right)$, where r_0 is the nominal range and ϕ_f is the beam deflection angle. We can confirm this effect by simply applying the same angular jitter with the FSM as is measured for a flame. As shown in Figure 6c) and d), the standard deviation (precision) of the range measurements increases from 2.5 µm to 4 µm for our measured flame-induced angular jitter of $\sigma(\phi_f)$ = 0.1 mrad, corresponding to a target slant of $\phi_t = 85°$ and r_0 = 0.4 m. In addition, the measured range distributions deviate from a normal distribution and show extended tails, which cannot be explained on geometrical grounds. These extended tails are explained by speckle phase noise, which is caused by the beam spot moving on the diffusely scattering surface [18]. Finally, as seen in Figure 6c), additional structure is present in the range measurement through the methane flame as compared to the FSM-jitter

beam deflection. This structure is caused by the 'flickering of the flame' and will be discussed in section 5C below.

B. Ranging offset in presence of flame

In addition to increased uncertainty, there can be overall range offsets induced by the flame. Figure 7a) shows range measurements to the diffusely scattering aluminum target through an intermittent methane (or acetylene) flame. After the burner is ignited, the measured range slowly increases at ~ 85 nm /s until reaching a steady state. Once the flame is extinguished, the range measurements slowly decrease again over several minutes, returning to the pre-flame distance. This behavior is consistent with the expansion of the optical table caused by heating. Furthermore, the SNR on the ranging signal decreases when the flame is present (Figure 7a)). These effects are even stronger for acetylene, which is consistent with the higher temperature and higher soot content of the acetylene flame (see also section 5C).

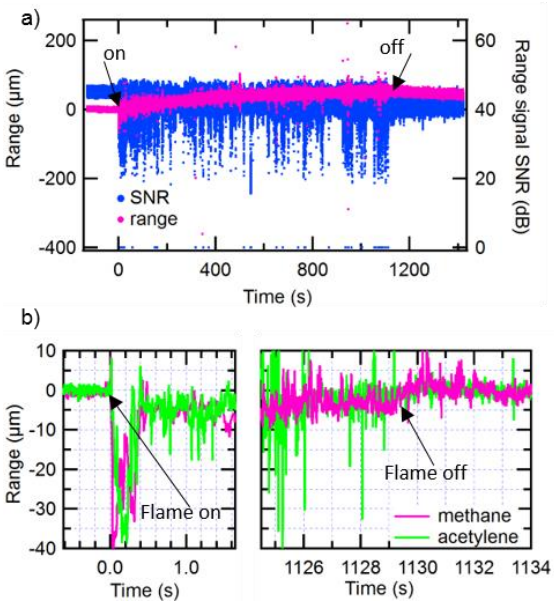

Figure 7: Ranging with fixed FSM position using the setup shown in Figure 1a) through a flame to an aluminum block at 2 m stand-off distance (the mean distance is subtracted from the plotted range). a) Measured range and SNR of the range signal acquired through a methane flame that is ignited at 0 s and extinguished at 1100 s. There is a slow range drift of initially 85 nm/s, that is attributed to thermal expansion of the experimental setup. b) Details showing the flame ignition (left panel) and extinction (right panel) events for both acetylene and methane flames. Traces in b) are smoothed with a 10-point binomial filter.

In addition to the slow thermal expansion of the optical table, we observe much faster range changes associated with a temperature-induced change in the air's index of refraction. As shown in the left panel of Figure 7b), the measured range decreases by -30 μm to -40 μm the moment the flame is lit for about 300 ms, which corresponds to the typical timescale associated with initial flame and flow instability. The range then stabilizes at about 5 μm below the pre-flame value. Once the flame is extinguished, there is an equivalent 5 μm range increase (right panel of Figure 7b)). However, because it takes significantly longer for the air to cool down, this range increase is slower and thus visually less obvious, especially for the noisier acetylene flame. The 5 μm step corresponds to a 100 ppm refractive index change across the ~50 mm thick flame, which is in good agreement with literature [19].

C. Ranging stability and precision in the presence of turbulent flames

As evident in Figure 6c), there is additional low-frequency noise structure present when ranging through a flame. To understand this, we analyze the fluctuations by both the PSD and Allan deviation. Figure 8 shows PSDs for range measured through methane and acetylene flames and with no flame (measurements are taken without scanning). In the case of methane, the noise floor increases for frequencies below 200 Hz and a distinct peak around 10 Hz is visible, coincident with natural flickering frequencies of diffusion flames due to Kelvin-Helmholtz type instabilities [20]. The buoyancy stretches the flame and quenching is observed at the center, which can result in detachment of the flame from the burner, leaving only a small flame at the burner's base. Vortices are formed as fresh non-reacting air is entrained into the flame [21,22]. In the time-domain range signal, the peak-to-peak excursion of the 10 Hz range oscillation is on the order of 3 μm to 7 μm, and can be explained by the above described flame instability oscillation which causes the

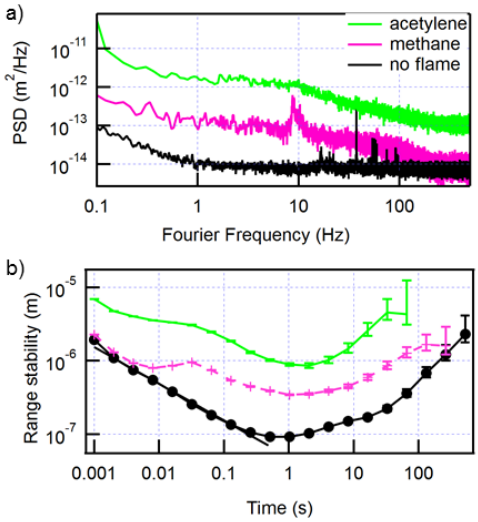

Figure 8: a) Power spectral density (PSD) of range measurements when ranging through an acetylene flame, a methane flame and not through the flame, with the FSM held at a fixed position. The peak near 10 Hz is cause by flame flickering and the peaks between 50 Hz and 60 Hz are caused by the FSM. b) Ranging stability (overlapping modified Allan deviation) while ranging to the brushed aluminum target at 2-meter stand-off and fixed position FSM. When there is no flame present (black) the stability averages down with $1/t^{1/2}$, (black line) to 100 nm. The range stability deteriorates in the presence of a methane flame (pink) and even more so for an acetylene flame (green). While ranging through the flame, an overall slope was removed from the range measurements before calculating the modified Allan deviation.

ranging light to alternately pass through cold air and hot flame, hence changing the optical path length due to refractive index change. This range excursion is consistent with the 5 μm step observed when the flame is first lit (see Figure 7b)). This distinct 10 Hz oscillation is also apparent in the range signal amplitude measurements, with excursions between 2 dB and 4 dB.

Figure 8b) depicts the ranging stability under the same range of conditions. In the absence of a flame the ranging precision averages down as $1/\sqrt{\text{averaging time}}$, until it reaches 100 nm at 1 second and is ultimately limited by the knowledge of the refractive index, comparable to other similar FMCW systems [15]. At time intervals longer than 1 s, the precision deteriorates due to slow drifts. When ranging through a flame, the 10 Hz flame flickering causes a worsening of the precision around 0.03 s averaging time. In all cases, a ranging stability (drift) of 5 μm or better is achievable for 100-second-long measurements. This is sufficient for a framerate to capture deforming structural objects. The range precision is 350 nm at 1 second averaging for the methane flame and 860 nm for acetylene. Even when ranging through the tip of the methane flame, where turbulence intensity is

largest [11], an averaged range precision of 700 nm is achieved at 4 seconds (not shown).

D. Impact of methane and acetylene flames on FMCW LADAR: summary

Table 1 summarizes the FMCW LADAR ranging precisions and signal loss (mostly dominated by soot in the flame) for a scanning system with at least 50 % oversampling to avoid moving speckle noise [15]. The standard deviation is obtained across 430 range measurements from a cross-section in the flat section of the step-block above the NIST logo, after a small slant in the x/y plane was removed.

The actual surface roughness and flatness of the aluminum block contributes to the stated precision and increases the measured precision in the absence of flames to 20 µm for a scanning FSM compared to the 2-3 µm precision measured for a fixed position FSM. When ranging through the methane flame, the combined precision remains dominated by this surface shape and still equals 20 µm. For an acetylene flame, the effects of beam deflection becomes noticeable and the precision deteriorates to 31 µm. Subtracting the no-flame precision in quadrature gives an additional acetylene flame induced uncertainty of 24 µm.

Table 1: Ranging precision from cross-sections taken from xyz 3D point clouds of the step-block, while ranging through methane or acetylene flames.

Measurement	3D-cross-section precision	Additional masked points due to flame (<30 dB SNR)
No flame	20 µm	0 %
Methane	20 µm	< 1 %
Acetylene	31 µm	1 % to 1.4 %

The increased ranging noise while mapping a surface through an acetylene flame compared to a methane flame is explained as follows. The adiabatic temperature of an acetylene flame is approximately 500 °C hotter than that of a methane flame [23], leading to a higher refractive index change and thus larger beam deflections. Additionally, acetylene has an atomic hydrogen to carbon (H/C) ratio of 0.08 compared to 0.34 for methane, resulting in a sootier flame [24]. Both the larger beam-deflection angle in conjunction with a small tilt of the target relative to the measurement beam as well as signal attenuation and scattering due to increased soot (see also ranging traces in Figure 7 and Figure 8) lead to poorer range precision. The increased soot in the acetylene flame also explains the slight decrease in ranging signal (between 1 % and 1.4 % of measurements are below 30dB, compared to less than 1 % when mapping through a methane flame).

In conclusion, we find that the effect of a clean-burning methane flame on FMCW LADAR is barely noticeable at the investigated flame size. Even for the sootier acetylene flame, the amount of invalid range measurements only increases to ~2 % and the achievable range precision is still 30 µm.

6. Scale-up experiments with wider burner

So far, all measurements were taken with the ranging beam traveling through a ~50-mm thick flame. To investigate beam deflection caused by thicker flames, we setup three 0.3 m thick natural gas burners (fuel > 90 % methane). Instead of the infrared FMCW laser, 405 nm blue laser light traverses the flames and is imaged using a camera placed 1 m behind Burner 1, see configuration in Figure 9a). As before, the x/y beam deflection is extracted from camera images.

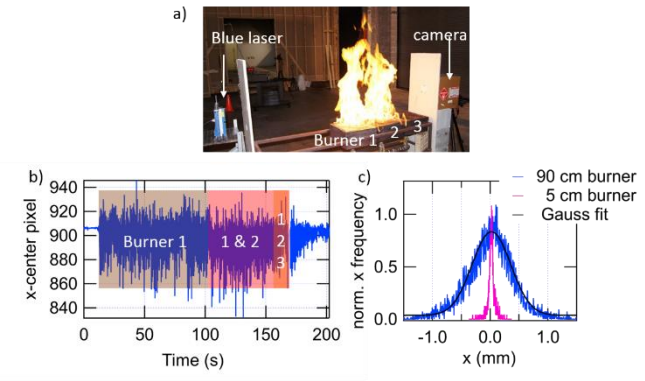

Figure 9: a) Photo of setup to measure beam-deflection through thick flames. b) Extracted beam center pixel x-position (the y-position behaves very similarly and is not shown). The first 0.3 m burner is ignited at 12 s. At 103 s and 165 s, the second burner and third burner are ignited, increasing the flame width first to 0.6 m and finally to 0.9 m. c) Blue trace: distribution of beam x-position for beam deflection measurements between 12 s and 170 s. The distribution is calculated after removing a low-order polynomial baseline from the data in b). Black: Gaussian fit. For comparison, the beam deflection distribution of the FMWC laser light traversing a ~50-mm methane flame is shown in pink.

When the burner closest to the laser source is ignited, the beam deviation at the camera has a standard deviation of 350 µm and a maximum deviation of ±2 mm, corresponding to a ±2 mrad beam deflection angle. Igniting the other two burners, hence tripling the flame width, doesn't significantly increase the beam deviation. Thicker flames, however, do increase beam attenuation due to soot, which along with the brighter background radiation of the flames themselves makes it harder to extract the beam position on the camera. Indeed, it was observed previously that the maximum beam deflection angle through a flame can be invariant with flame size [19] and that the beam deviation increases proportionally to the distance between the first flame front encountered by the laser and the target. This angular deflection is only a factor of three greater than that encountered with the smaller flame and would yield a single measurement range precision of 35 µm for the same target. Further, we found no significant offset in the beam deviation, indicating that also for thick flames, the precision could improve through temporal averaging [11].

7. Edge tracking

To track the movement of well-defined features, it is often not necessary to capture a complete 3D image. Figure 10 shows an example of a single L-scan pattern (green), capable of tracking the position of an edge (the 100 µm high vertical step of the aluminum step-block). We choose a > 50 % beam overlap to reduce moving speckle noise. The step-block is translated along the x-axis with a constant nominal velocity of 0.5 mm/s, which was selected to match critical element deformation speeds in structural fire tests. From the known scanning pattern, we assign a time and location to the 100 µm step for each crossing, as shown in Figure 10b). A linear fit to the extracted step x-location over time yields a slope of 0.517 ±0.004 mm/s , close to the nominal speed of 0.5 mm/s.

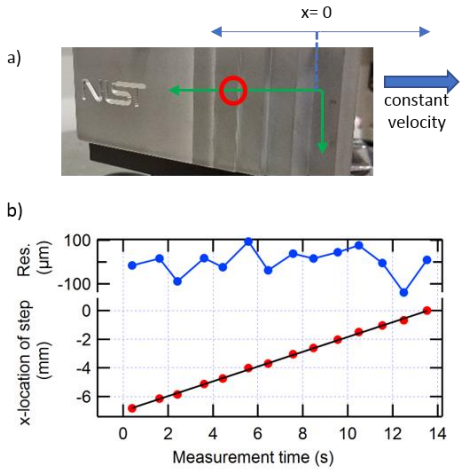

Figure 10: Tracking a moving object. a) The block is placed on a lateral translation stage moving at constant velocity. The tracked step is circled in red and the scanning pattern is sketched in green. b) Extracted x-location of the step as a function of measurement time. Also shown are a linear fit and residuals.

The above edge tracking is shown for possible lateral motion in the x/y plane. If the object also moves/deforms fast in the z-direction, the FMCW LADAR range would be affected by Doppler shifts. For FMCW systems this Doppler effect is removed by averaged measurements taken at alternating positive and negative chirps.

8. Conclusions and outlook

The influence of flames on dimensional measurements of moving and deforming objects in structural fire research was investigated, specifically regarding the use of coherent laser ranging in the form of frequency modulated continuous wave laser detection and ranging (FMCW LADAR). We show that FMWC LADAR can capture deforming shapes through flames. The heterodyne gain enables measurements at low return signals and masks out most of the flame's background radiation, while the fast update rate makes the system somewhat immune against signal distortion induced by turbulent thermal gradients of diffusion flames. We show that the increase in ranging uncertainty for diffusely scattering surface through fire is primarily caused by flame-induced beam deflections. Preliminary studies show that the first layer of flame traversed by the ranging beam dominates the angular beam deflection, which should enable the application of FMCW LADAR to larger scale fires and objects.

Acknowledgement. We thank Brian Simonds, Matthew Bundy, Nazanin Hoghooghi, and Amanda Makowiecki for technical assistance and review of this manuscript.

REFERENCES

[1] W.L. Grosshandler, "Fire Resistance Determination & Performance Prediction Research Needs Workshop: Proceedings," NIST Interagency/Internal Report (NISTIR) - 6890. (2002).

[2] J. Beitel, "Analysis of Needs and Existing Capabilities for Full-Scale Fire Resistance Testing," Grant/Contract Reports (NISTGCR) -. (2008).

[3] K.H. Almand, Structural Fire Resistance Experimental Research: Priority Needs of U.S. Industry, Springer Science & Business Media, 2013.

[4] V.K.R. Kodur, M. Garlock, N. Iwankiw, "Structures in Fire: State-of-the-Art, Research and Training Needs," Fire Technol., **48**, 825–839 (2012).

[5] L. Bisby, J. Gales, C. Maluk, "A contemporary review of large-scale non-standard structural fire testing," Fire Science Reviews. **2**, 1 (2013).

[6] T. McAllister, W. Luecke, M. Iadicola, M. Bundy, Measurement of Temperature, Displacement, and Strain in Structural Components Subject to Fire Effects: Concepts and Candidate Approaches, National Institute of Standards and Technology, Gaithersburg, MD, 2012.

[7] K. Harding, Handbook of Optical Dimensional Metrology, CRC Press, 2013.

[8] W.C. Stone, M. Juberts, N. Dagalakis, J. Stone, J. Gorman, Performance Analysis of Next-Generation LADAR for Manufacturing, Construction, and Mobility, NIST Construction Metrology and Automation Group, 2004.

[9] G. Berkovic, E. Shafir, "Optical methods for distance and displacement measurements," Adv. Opt. Photon. **4**, 441–471 (2012).

[10] F. Willomitzer, G. Häusler, "Single-shot 3D motion picture camera with a dense point cloud," Opt. Express, **25**, 23451–23464 (2017).

[11] M.S. Hoehler, C.M. Smith, "Application of blue laser triangulation sensors for displacement measurement through fire," Meas. Sci. Technol. **27**, 115201 (2016).

[12] M. Locatelli, E. Pugliese, M. Paturzo, V. Bianco, A. Finizio, A. Pelagotti, P. Poggi, L. Miccio, R. Meucci, P. Ferraro, "Imaging live humans through smoke and flames using far-infrared digital holography," Opt. Express, **21**, 5379–5390 (2013).

[13] M.-C. Amann, T. Bosch, M. Lescure, R. Myllyla, M. Rioux, "Laser ranging: a critical review of usual techniques for distance measurement," Opt. Eng. **40**, 10–19 (2001).

[14] P.A. Roos, R.R. Reibel, T. Berg, B. Kaylor, Z.W. Barber, W.R. Babbitt, "Ultrabroadband optical chirp linearization for precision metrology applications," Opt. Lett. **34**, 3692–3694 (2009).

[15] E. Baumann, F.R. Giorgetta, J.-D. Deschênes, W.C. Swann, I. Coddington, N.R. Newbury, "Comb-calibrated laser ranging for three-dimensional surface profiling with micrometer-level precision at a distance," Opt. Express. **22**, 24914–24928 (2014).

[16] T. DiLazaro, G. Nehmetallah, "Large-volume, low-cost, high-precision FMCW tomography using stitched DFBs," Opt. Express, **26**, 2891–2904 (2018).

[17] Z. Wang, B. Potsaid, L. Chen, C. Doerr, H.-C. Lee, T. Nielson, V. Jayaraman, A.E. Cable, E. Swanson, J.G. Fujimoto, "Cubic meter volume optical coherence tomography," Optica, **3**, 1496–1503 (2016).

[18] E. Baumann, J.-D. Deschênes, F.R. Giorgetta, W.C. Swann, I. Coddington, N.R. Newbury, "Speckle phase noise in coherent laser ranging: fundamental precision limitations," Opt. Lett. **39**, 4776–4779 (2014).

[19] G.W. Faris, R.L. Byer, "Beam-deflection optical tomography of a flame," Opt. Lett.,. **12**, 155–157 (1987).

[20] J. Buckmaster, N. Peters, "The infinite candle and its stability—A paradigm for flickering diffusion flames," Symposium (International) on Combustion. **21**, 1829–1836 (1988).

[21] N. Yilmaz, A.B. Donaldson, W. Gill, R.E. Lucero, "Imaging of flame behavior in flickering methane/air diffusion flames," J Vis. **12**, 47–55 (2009).

[22] L.W. Kostiuk, R.K. Cheng, "The coupling of conical wrinkled laminar flames with gravity," Combustion and Flame. **103**, 27–40 (1995).

[23] I. Glassman, R.A. Yetter, N.G. Glumac, Combustion, Academic Press, 2014.

[24] Z.G. Habib, P. Vervisch, "On The Refractive Index of Soot at Flame Temperature," Combustion Science and Technology. **59**, 261–274 (1988).